Global Climate Diagnosis in a Linear Stochastically Forced Framework

Prashant D. Sardeshmukh

CIRES Climate Diagnostics Center, University of Colorado, and
NOAA Earth System Research Laboratory, Boulder, Colorado

The governing equations for weather and climate evolution are obviously nonlinear. However, in many contexts the evolution of anomalies (departures from a background state) is found to be consistent with deterministically linear and stochastically perturbed dynamics of the form

$$\frac{dx}{dt} = A\,x + f_{ext} + B\,\eta - D , \qquad (1)$$

where $x(t)$ is an N-component anomaly state vector, $f_{ext}(t)$ is an N-component external forcing vector, η is an M-component noise vector of independent Gaussian white noise components with zero expected mean, $A(t)$ and $B(x,t)$ are NxN and NxM matrices, and $D(t) = <B\eta>$ is an N-component expected mean noise forcing vector, which is zero if B does not depend on x. The equations for all classical free and forced linear wave dynamics in the climate system may be expressed as special cases of this general form, as may also the equations for the evolution of small amplitude forecast errors, important in modern data assimilation techniques. The traditional use of linear models in such contexts has advanced both basic understanding and practical applications, but has stopped short of claiming that observed full-amplitude anomalies also obey such equations. Evidence has steadily accumulated, however, to support even this latter stronger claim, especially for "coarse-grained" anomalies averaged over various time and space scales. The claim is also consistent with the evident "red noise" character of much of observed climate variability. Indeed, Eq. (1) primarily represents a generalization of the univariate linear Markov (i.e. red noise) model to a multivariate model with external forcing and time varying system parameters. Its approximate validity suggests that the coarse-grained nonlinear tendency terms in the governing equations, associated primarily with fluxes by unresolved eddies, can in principle be linearly parameterized in terms of the coarse-grained anomalies x, and the unparameterized remainder can be treated as stochastic white noise. This means, importantly, that the matrix A in (1) is in general not that obtained by directly linearizing the governing equations but also includes such linear flux parameterizations, and the matrix B accounts for the amplitude and correlation structure of the unparameterized remainder as a "stochastic parameterization".

As discussed by Sardeshmukh and Sura (2009), the approximation (1) has been shown to be valid by many investigators in widely different contexts, and useful for both diagnosis and prediction. We reiterate that it does not ignore the chaotic nonlinearities of the underlying system but rather treats them as stochastic white noise, of finite amplitude. The basic assumption made in (1) is not that the chaotic nonlinear terms are small, but that their temporal correlation scales are much shorter than those of the linear terms. In the limit of infinitely short correlation scales, such terms can be

rigorously treated as a stochastic forcing of x. In this limit the equations for the statistical moments of x in (1) are both linear and closed, i.e. the equations for the higher moments involve moments of the same or lower order, which obviates the need for closure assumptions as made in turbulence modeling to derive those moments. This has important implications for probabilistic climate and weather prediction. For example, the linearity of the equation for the first moment, i.e. the expected mean $<x>$ of x, implies that $<x>$ responds linearly to external forcing, and the expected mean $<x(t)|x(0)>$ of $x(t)$ given $x(0)$ is a linear prediction. Sardeshmukh and Sura (2009) also made the important point that (1) can generate realistic non-Gaussian statistics of x without compromising the linear and closed character of the moment equations if B is allowed to depend linearly on x. In this case the expected mean noise vector $D(t)$ is not zero, but can nevertheless be explicitly related (again, without making closure assumptions) to the x-independent ("additive" noise) and x-dependent ("multiplicative" noise) parts of $B\eta$.

It is not our intent here to present an exhaustive treatment of (1) and all its implications. Rather, we provide a few illustrations of its validity and utility in some atmospheric and oceanic contexts of relevance to ECMWF. To that end we restrict ourselves to the simplest case of constant deterministic and stochastic system parameters A and B and no external forcing in (1), discussed at length e.g. by Penland (1989), Penland and Ghil (1993), Penland and Matrosova (1994), and Penland and Sardeshmukh (1995). It can be shown that x then has Gaussian statistics, and

$$< x > \quad = \quad 0 \tag{2a}$$

$$x(t+\tau) \quad = \quad e^{A\tau} x(t) + \varepsilon \ = \ G(\tau) x(t) \ + \ \varepsilon \tag{2b}$$

$$E(\tau) \quad = \quad <\varepsilon\, \varepsilon^T> \quad = \quad C(0) \ - \ G(\tau)\, C(0)\, G^T(\tau) \tag{2c}$$

$$C(\tau) \quad = \quad e^{A\tau} C(0) \quad = \quad G(\tau)\, C(0) \tag{2d}$$

$$0 \quad = \quad A\, C(0) \ + \ C(0)\, A^T \ + \ B\, B^T \tag{2e}$$

where $C_{ij}(\tau) = <x_i(t+\tau)\, x_j(t)>$ defines the time-lag covariance matrices $C(\tau)$. Equation (2b), which can readily be derived from (1), is a prediction equation for $x\,(t+\tau)$ given $x(t)$, with an expected forecast mean $\exp(A\tau) x(t)$ and a forecast error ε whose covariance as a function of the forecast lead time τ is given by (2c). Because x is Gaussian, its statistics are characterized completely by its first and second moments, and so (2b) and (2c) are sufficient for providing complete probabilistic forecast information of the system. Identifying $G(\tau) x(t)$ in (2b) with the predictable forecast signal, and ε with the unpredictable noise, also enables one to investigate system predictability in terms of the signal-to-noise ratio $Tr\, [\, G\, C(0)\, G^T\,]\, /\, Tr\, E$ as a function of τ. Equation (2d) is readily derived from (2b). Equation (2e) is the covariance budget of x in a statistically stationary state. Because $C(0)$ and BB^T are both positive-definite, (2e) can be satisfied only if A is a stable operator, i.e. only if its eigenvalues have negative real parts. This means that the domain-integrated forecast error variance $Tr\, E$ increases monotonically in (2c) from 0 at $\tau = 0$ to $Tr\, C(0)$ at $\tau = \infty$. However, it does *not* mean that the magnitude of the forecast signal $G(\tau) x(t)$ always decreases monotonically with τ. This is because the singular values of G (i.e. the square root of the eigenvalues of $G^T G$) can be larger than 1 over a range of τ even if A is stable, and if $x(0)$ projects on the associated singular vectors, then the forecast signal can grow over that forecast range before eventually decaying to zero. In such forecast cases the system is more predictable than on average, and the cases can be identified *a priori*.

An extremely useful practical application of (2) is that it allows one to build a "Linear Inverse Model" (LIM) of a system, i.e. to estimate the matrices A and B, directly from the observed zero-lag and time-lag covariance statistics of the system. Specifically, knowledge of $C(0)$ and $C(\tau_0)$ at some specified lag τ_0 is sufficient to deduce A from (2d), and then to deduce B from (2e). [Strictly speaking, this only yields BB^T, not B itself, which is uniquely determined only up to an arbitrary unitary matrix multiplier. However, using B in (1) with such an arbitrary multiplier makes no difference to either the marginal or the conditional probabilities of x, as is evident from (2e) and (2c)]. If (1) is a good approximation to the anomaly dynamics, then this procedure should yield the same A regardless of the choice of the training lag τ_0. This is the so-called "Tau Test" of Penland and Sardeshmukh (1995) for demonstrating the validity of (1). The test can also be formulated in other equivalent ways, such as requiring that the $C(\tau)$ matrices "predicted" at all lags using (2d) and the A derived from $C(\tau_0)$ should match the observed $C(\tau)$ matrices, or that the power spectra of x based on such predicted $C(\tau)$ matrices should match the observed power spectra.

Before proceeding to specific examples, we note an attractive property of (1), that it is isomorphic with respect to linear invertible transformations of the state vector x. In other words, if the dynamics of x are established as linear and stochastically forced in any one particular space (grid space, spherical harmonic space, EOF space, etc.) then they are also established as linear and stochastically forced in all other such related spaces. This property is useful for building a LIM in a relatively low-dimensional space, such as a truncated EOF space, and then transforming the results to grid space for display and interpretation.

Subseasonal Atmospheric Variability

Our first example is a LIM of subseasonal extratropical and tropical atmospheric variations in the northern winter, constructed and analyzed in detail by Newman and Sardeshmukh (2008). The focus is on the variability of 7-day running mean anomalies from the annual cycle over a 35-yr period (1968-2003). The state vector x is an 86-component vector, whose components are the amplitude coefficients (i.e. Principal Components or PCs) of the leading 40 combined EOFs of upper (250 hpa) and lower (750 hpa) tropospheric extratropical streamfunction, 24 EOFs of extratropical sea level pressure, 18 EOFs of column-integrated tropical diabatic heating, and 4 EOFs of extratropical stratospheric (30 hpa) streamfunction, explaining about 90%, 90%, 55%, and 84% of the variability of these fields. Newman and Sardeshmukh (2008) estimated the matrix A in (1) using $C(0)$ and $C(\tau_0 = 5 \text{ days})$ in Eq. (2d), and then used it to "predict" the $C(\tau)$ for other lags. Figure 1 shows a comparison of the observed and predicted $C(\tau_0 = 21 \text{ days})$. The quantities compared are the local 21-day lag covariances of 250 hpa streamfunction (upper panels), sea level pressure (middle panels), and tropical heating (lower panels) anomalies. The agreement of the predicted and observed values is generally excellent.

Newman and Sardeshmukh (2008) used this encouraging demonstration of linearity to justify investigating the relative impacts of tropical heating and stratospheric circulation anomalies on the extratropical tropospheric anomalies by switching off appropriate elements of the A matrix and recomputing $C(\tau_0 = 21 \text{ days})$ using (2d), and also assessing the impacts on $C(0)$ itself using (2e). This analysis showed that tropical diabatic heating greatly enhances $C(\tau_0 = 21 \text{ days})$ over most of the

Northern Hemisphere, especially over the Pacific and North America. The stratospheric contribution is largely confined to the polar region, where it ensures that the dominant pattern of sea level pressure variability is the annular Arctic Oscillation rather than the more localized North Atlantic Oscillation. Over the North Atlantic, both contributions are important, although some of the stratospheric influence is ultimately traceable to tropical forcing.
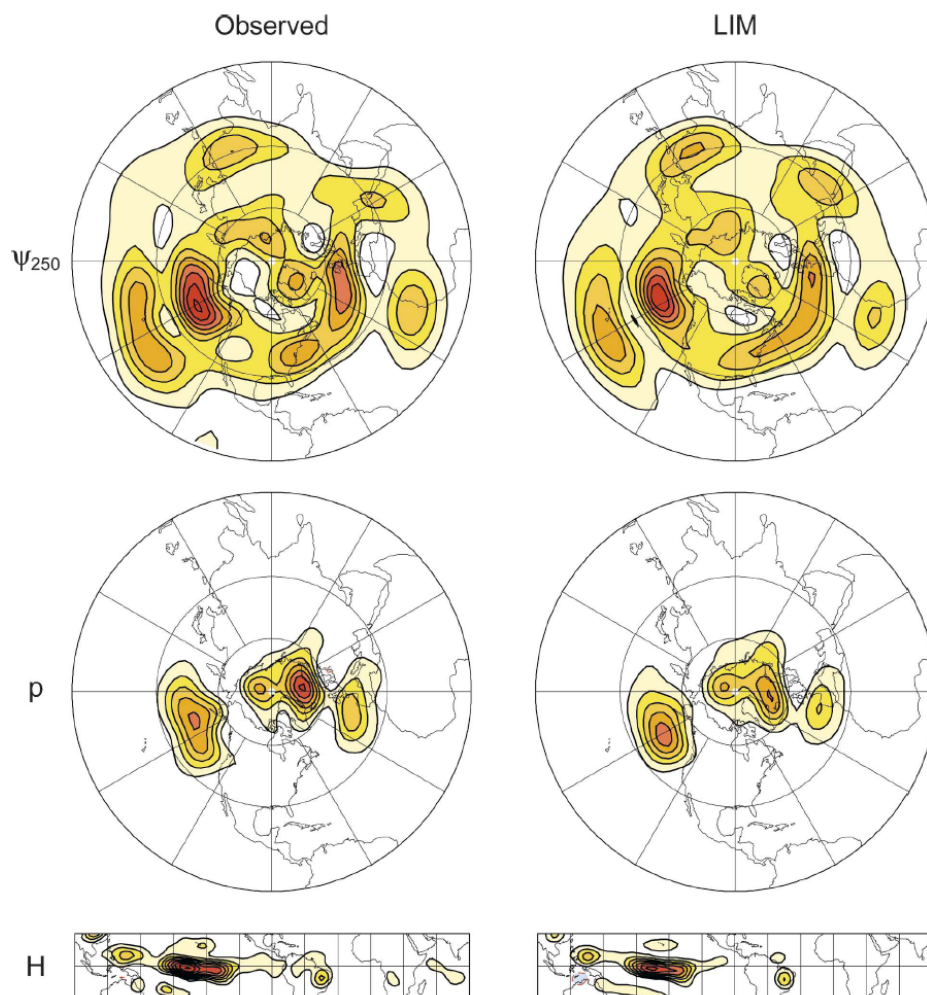

*Figure 1: Observed (left panels) and LIM-predicted (right panels) 21-day lag-covariance. Top panels: 250 hPa streamfunction (ψ_{250}) (contour/shading interval = 10^{13} m^4s^{-2}). Middle panels: sea level pressure (**p**) (contour/shading interval = 50000 Pa^2). Bottom panels: diabatic heating (H) (contour/shading interval = 0.1 $Pa^2K^2s^{-2}$). Orange/red shading represents positive values, and blue shading represents negative values. From Newman and Sardeshmukh (2008).*

Forecasting Week 3 Forecast Skill

Our second example of the utility of (1) is a LIM of wintertime 7-day running mean anomalies, developed by Winkler et al (2001) and Newman et al (2003), that can successfully identify relatively skillful Week 3 forecast cases of extratropical streamfunction anomalies *a priori*. This LIM is similar to but simpler than that developed later by Newman and Sardeshmukh (2008). The state vector *x* is a 37-component vector whose components are the PCs of the leading 30 combined EOFs of upper (250 hpa) and lower (750 hpa) tropospheric extratropical streamfunction and 7 EOFs of column-integrated tropical diabatic heating anomalies. The matrix *A* in (1) was estimated using *C*(0) and

$C(\tau_0 = 5$ days$)$ in Eq. (2d). Using this A, the system propagator matrices $G(\tau) = \exp(A\tau)$ were determined over a range of τ, and their singular vectors were calculated. As mentioned earlier, a relatively large initial state projection on the leading singular vectors of G can be used to identify relatively skillful forecast cases *a priori*. This was done using the three leading singular vectors of $G(\tau_0 = 21$ days$)$. Figure 2 shows comparisons of the expected and actual Week 3 forecast skill of 250 mb extratropical streamfunction for 8 different categories of the initial state projection on these singular vectors, ranging from a low projection on all three SVs (shown at the right end of the plot) that occurred in 32% of all the forecast cases considered, to a high projection on all three SVs (the left end of the plot), that occured in 6% of the cases. The LIM's actual skill is clearly consistent with the predicted skill based on these projections. It is interesting that the variation of skill among these forecast categories of a 1998 version of NCEP's Medium Range Forecast (MRF) model is also consistent with the LIM's predicted skill variation. This suggests that such simple LIMs might prove useful in forecasting the forecast skill of even state-of-the-art comprehensive NWP models.
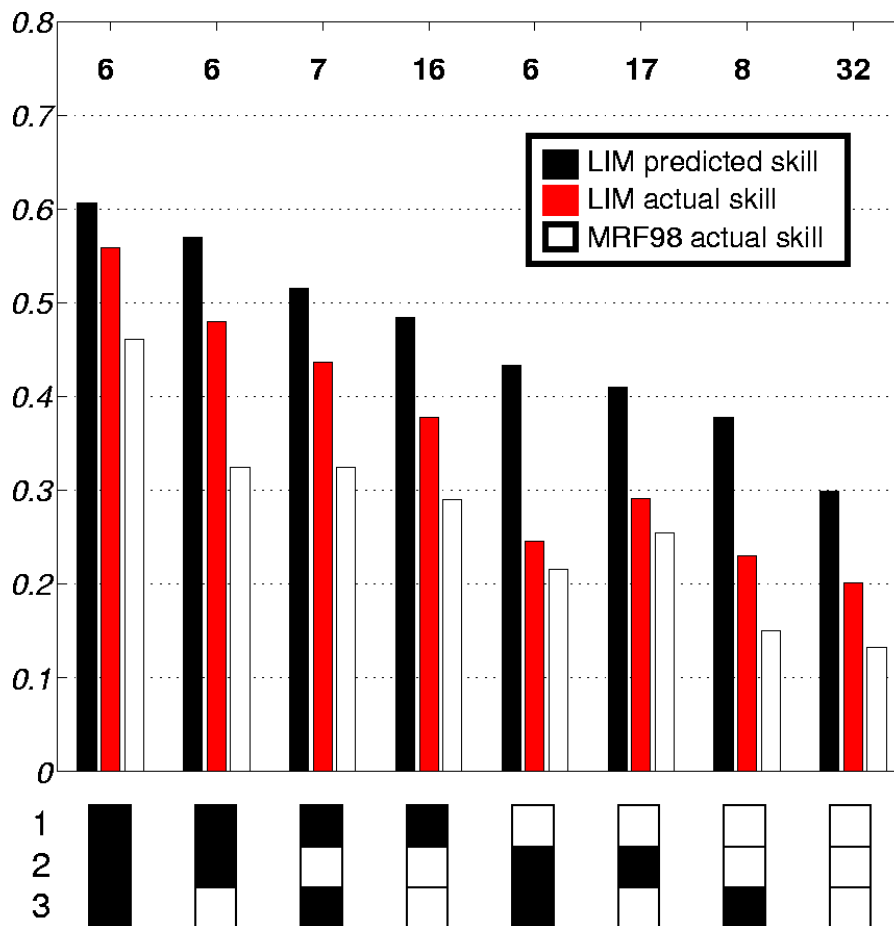

Figure 2. Expected *and* actual *pattern correlation skill of Week 3 wintertime Northern Hemisphere forecasts of 250 hpa streamfunction, stratified by initial state projections on the right singular vectors of G (τ =21 days). The figure shows that the singular vectors of the empirically estimated G(τ) = exp(Aτ) operator can help identify relatively more skillful cases* a priori. *From Newman et al 2003.*

Tropical SST variability

Although the general "red noise" character of the power spectra of many climate variables has often been noted, it is only gradually being appreciated that the red noise processes contributing to the low-frequency tails of those spectra can have much shorter correlation scales. Indeed, recognition of the fact that relatively rapid physical processes can influence longterm climate variability is at the heart of the current interest in "seamless" approaches to weather and climate prediction. Simple generalizations of the univariate red noise model, as in (1), are entirely consistent with such "multi-scale interactions". Figure 3 provides an example. It shows the power spectra of the projections of observed and IPCC/AR4 model-simulated monthly tropical SST anomaly fields on the dominant EOF pattern of observed SST variability during 1950-1999. The general red noise character is evident in both the observed and simulated spectra. However, many of the model spectra differ substantially from the observed spectrum, especially at low frequencies (note the log scales). Is this necessarily due to model errors in representing slow processes? A simple 47-component Coupled LIM of observed 7-day running mean tropical SST, tropical tropospheric circulation, and diabatic heating anomalies during 1982-2005 constructed by Newman, Sardeshmukh, and Penland (2009; henceforth NSP09) suggests otherwise. The state vector of this LIM has 20 PCs of SST, 7 of tropospheric streamfunction, 3 of velocity potential, and 17 of diabatic heating as its 47 components. The A matrix in (1) was estimated using $C(0)$ and $C(\tau_0 = 6 \text{ days})$ in (2d); this was then used to estimate B from (2e). A 100-member ensemble of 50-yr model runs using these A and B matrices in (1) was then generated. The thick blue curve in Figure 3 shows the ensemble-mean SST spectrum obtained in these runs, with the ensemble spread (95% confidence intervals) indicated by grey shading. It is remarkable how well even such a simple 47-component LIM, derived from the *6-day* lag covariances of 7-day running mean anomalies, captures the observed SST spectrum within the sampling error bars even at the lowest frequencies. This provides not only strong evidence in support of (1) in the tropics but also strongly suggests that the tropical SST spectrum at interannual and longer periods is determined primarily by processes with much shorter time scales, that evolve appreciably over intervals as short as a week. The LIM-derived sampling error bars are also useful for identifying those model spectra in Figure 3 whose deviations from the observed spectrum are statistically significant.

The importance of ocean-atmosphere coupling in ENSO and MJO evolution

NSP09 used the Coupled Tropical LIM described in the previous section to investigate this issue, following two different approaches. In the first approach, they modified the LIM's A matrix by switching off the elements linking the 20 SST and 27 atmospheric components of the 47-component state vector x, and generating a 100-member ensemble of 24-yr model runs using this decoupled A matrix (but retaining the original B matrix). The modified and original ensemble-mean LIM spectra of the leading PCs of SST and tropospheric diabatic heating are shown in the upper and lower panels of Figure 4, respectively, with the grey shading showing the ensemble spread (95% confidence intervals) obtained in the original runs. The corresponding observed spectra, depicted by the thick red curves, are well within these shaded sampling error bars. The effect of decoupling is dramatic on both the SST and diabatic heating spectra on interannual (ENSO) time scales, but is remarkably small on subseasonal (MJO) scales. This reconfirms that ENSO is a strongly coupled phenomenon, but also suggests that the MJO is mostly an internal atmospheric phenomenon that is only weakly coupled to SST.
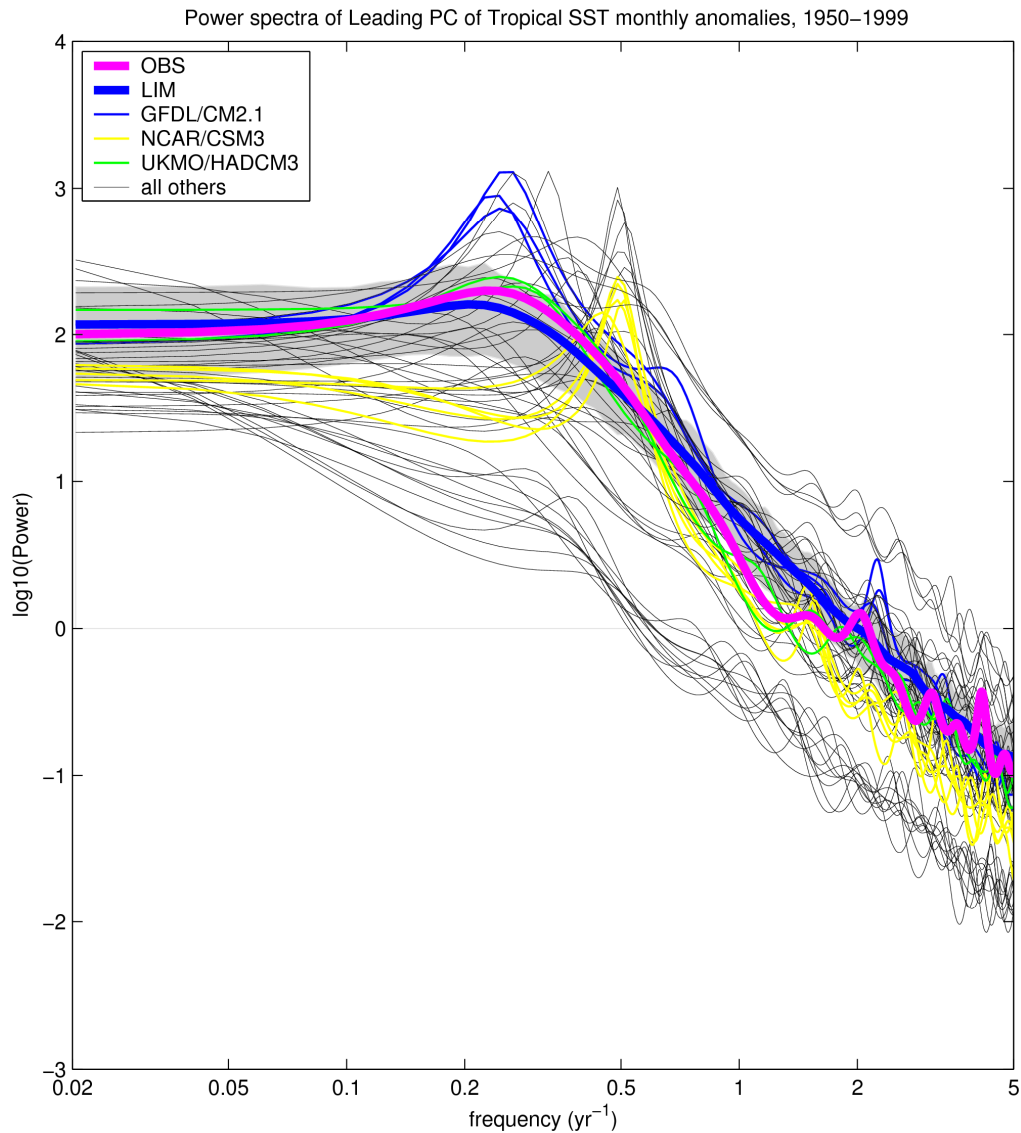
Figure 3: Spectra of the leading principal component (PC) of monthly tropical SST variability from observations (pink line) compared to spectra derived from the output of the Coupled LIM (blue line) and the "20th-century" (20c3m) IPCC AR4 coupled GCMs (thin black, yellow, blue, and green lines). The observed spectrum was computed from the time series of the leading PC as determined from an EOF analysis of monthly SST anomalies in the region between 25°S-25°N for the years 1950-1999. The Coupled LIM was constructed from weekly 1982-2005 data, and then a 100-member ensemble of 50-yr LIM model runs was made. For consistent comparison and because it is the real system these sophisticated models are trying to simulate, both the LIM and GCM output were projected onto the leading observed EOF of monthly anomalous SST to produce the PC time series in each model, for the same 1950-1999 period. Gray shading indicates the 95% confidence interval from the LIM, based on the spread of the 100 ensemble members. From Newman, Sardeshmukh, and Penland (2009).
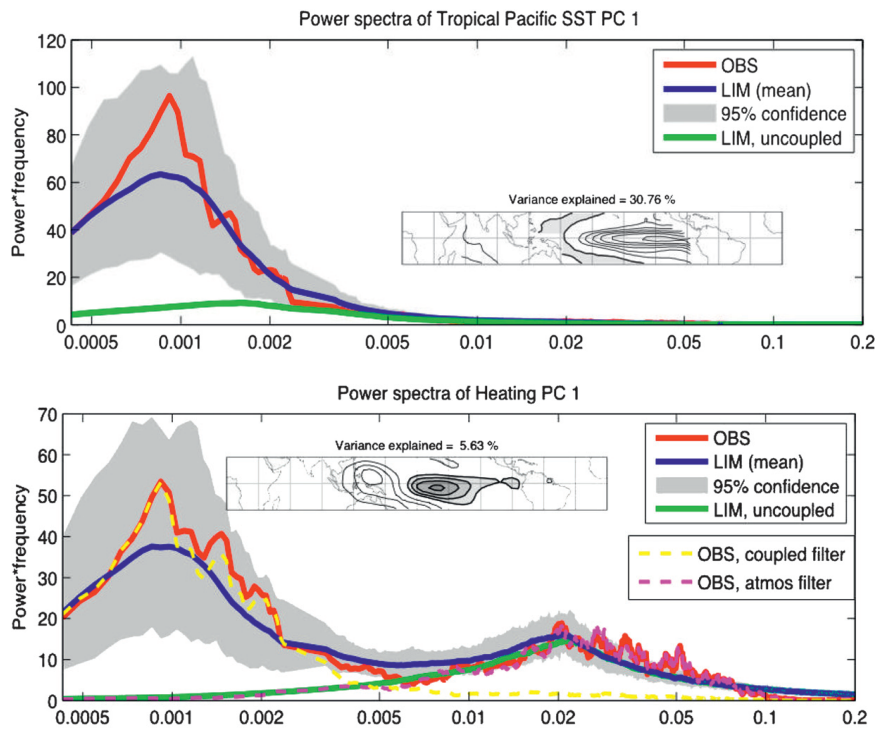
Figure 4: Observed power spectra of the leading Tropical SST and atmospheric diabatic heating EOFs (red curves), compared to spectra predicted by the Coupled LIM (blue curves) and by the Uncoupled LIM (green curves). Gray shading represents 95% confidence intervals determined from a 2400 yr run of the Coupled LIM. Insets in each panel show the corresponding EOF and the variance of weekly anomalies explained by that EOF. Dashed curves in the lower panel: spectra of the observed heating PC 1 projected onto the subset of either the "Coupled" (yellow) or "Internal" (pink) eigenmodes of the full LIM operator. Adapted from Newman et al (2009).

In their second approach, NSP09 examined the eigenmodes of the original system matrix *A,* and found that they separated remarkably cleanly into "Coupled" and "Internal Atmospheric" eigenmode categories with both strong atmospheric and SST components or just a strong atmospheric component, respectively. They then determined the amplitude time series of x(t) in these eigenmode spaces. The dashed yellow (dashed pink) curves in the lower panel of Figure 4 show the spectra of the diabatic heating PC1 in these coupled (internal) spaces. They show that the interannual variations of the heating project predominantly on the coupled eigenvectors, whereas the subseasonal variations project predominantly on the internal atmospheric eigenvectors, consistent with the conclusion drawn from the first approach.

Non-Gaussian statistics of daily atmospheric circulation and SST variability

As a final example of the validity and diagnostic utility of the linear stochastically forced approximation (1), we consider its ability to explain non-Gaussian aspects of the observed statistics. Sardeshmukh and Sura (2009) and Sura and Sardeshmukh (2008) recently provided striking evidence of non-Gaussianity in the statistics of daily observed SST and upper tropospheric vorticity variations, in terms of Skewness S and Excess Kurtosis K, reproduced in Figure 5 here. There are several remarkable features to note in these statistics: 1) the patterns of *S* and *K* are highly geographically coherent in both the atmosphere and the oceans, with relatively high magnitudes in the vicinity of strong atmospheric jets and ocean currents and in the tropical ENSO region, 2) both large positive and

large negative values of S tend to be associated with large positive values of K, and 3) this K-S relationship is a remarkably simple parabolic inequality, $K > 1.5 \, S^2$, as highlighted in the scatter plots of K versus S in the left panels. Sardeshmukh and Sura (2009) showed that non-zero values of S and K and also precisely this K-S relationship occur naturally even in a 1-component system of the form (1) in which B depends linearly on the system state x. The 1-component model also provides insight into how S depends sensitively on the correlation of the state-independent and state-dependent parts of the stochastic forcing $B\eta$, i.e on the so-called Correlated Additive and Multiplicative noise ("CAM" noise) forcing.

The magnitudes, geographical structures, and K-S relationships evident in Figure 5 have critical implications for GCMs and their ability to represent the statistics of extreme and high-impact weather events. This is because accurate representations of K and S are a necessary condition for accurately representing the tails of probability density functions (PDFs) and therefore the likelihoods of extreme values. For example, the statistics of extreme surface heat fluxes at the air-sea interface, that can have an important effect on hurricane statistics, depend sensitively on the statistics of extreme daily SST anomalies. If the models cannot reproduce Figure 5, their ability to represent extreme-event statistics will clearly be compromised.
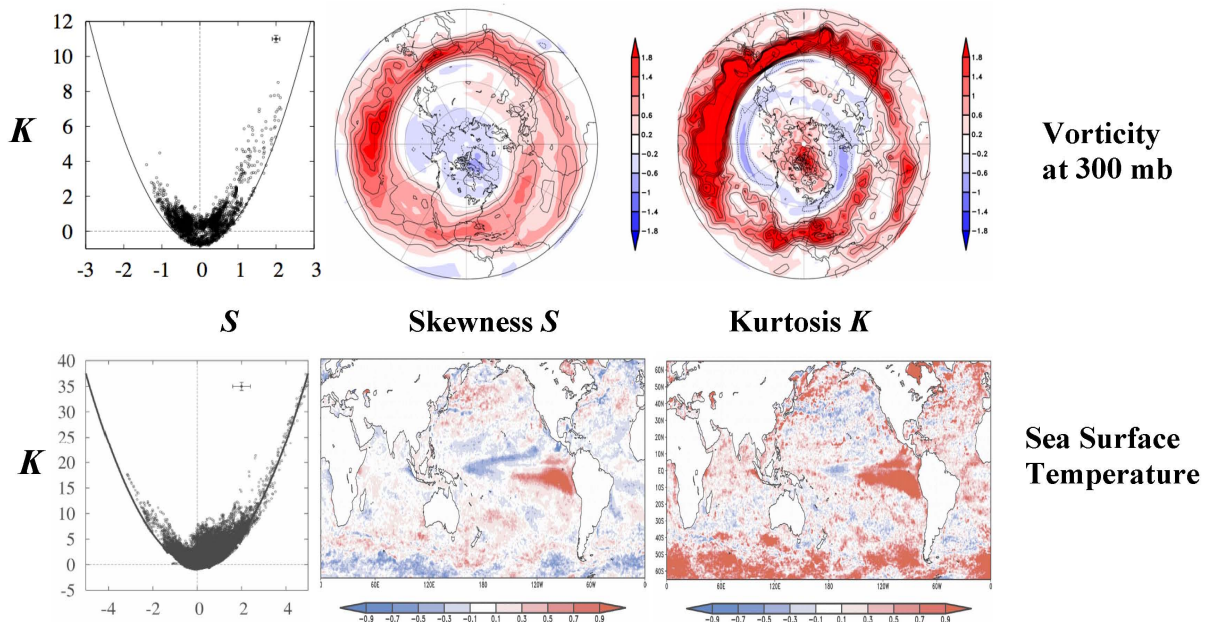

Figure 5: Upper Center and Right Panels: Observed Skewness S and excess Kurtosis K of daily 300 mb vorticity variations during the northern winters of 1970-99, estimated using the NCEP/NCAR reanalysis dataset. The fields are both colored and contoured for clarity. The contours are drawn at intervals of 0.4, starting at 0.2. Lower center and right panels : The S and K of daily SST variations during the winters of 1985-2006, estimated using the Reynolds et al (2007) dataset.

Left Panels: The S and K values from the center and right panels displayed in the form of scatterplots. The estimated 95% confidence intervals are indicated in the upper portions of the panels. The solid curve is a parabola $K = 1.5 \, S^2 - 0.6$ in the upper panel and $K = 1.5 \, S^2$ in the lower panel. From Sardeshmukh and Sura (2009) and Sura and Sardeshmukh (2008).

References

Newman, M., Sardeshmukh, P.D., Winkler, C.R., and J.S. Whitaker, 2003: A study of subseasonal predictability. Mon. Wea. Rev., 131, 1715-1732.

Newman, M., and P. D. Sardeshmukh, 2008: Tropical and Stratospheric Influences on Extratropical Short-Term Climate Variability. *J. Climate*. **21**, 17, 4326-4347.

Newman, M., Sardeshmukh, P.D., and C. Penland, 2009: How important is air-sea coupling   in ENSO and MJO evolution? *J. Climate*, **22**, 11, 2958-2977.

Penland, C., 1989: Random forcing and forecasting using principal oscillation pattern analysis. *Mon. Wea. Rev.*, **117**, 2165-2185.

Penland, C., 1996: A stochastic model of Indo-Pacific sea surface temperature anomalies. *Physica D*, 98, 534-558.

Penland, C., and M. Ghil, 1993: Forecasting northern-hemisphere 700-mb geopotential height anomalies using empirical normal-modes. *Mon. Wea. Rev.*, **121**, 2355-2372.

Penland, C., and L. Matrosova, 1994: A balance condition for stochastic numerical models with application to the El Niño–Southern Oscillation. *J. Climate., 7, 1352–1372*.

Penland, C., and P. D. Sardeshmukh, 1995: The optimal growth of tropical sea surface temperature anomalies. *J. Climate.*, **8***, 1999-2024.

Sardeshmukh, P.D., and P. Sura, 2009: Reconciling non-Gaussian climate statistics with linear dynamics. *J. Climate*, **22**, 5, 1193-1207.

Sura, P., and P.D. Sardeshmukh, 2008: A global view of non-Gaussian SST variability. J. Phys. Oceanography, **38**, 3, 639-647.

Winkler, C. R., M. Newman, and P. D. Sardeshmukh, 2001: A linear model of wintertime low-frequency variability. Part I: Formulation and forecast skill. *J. Climate*, **14**, 4474-4494.